OPEN ACCESS
IOP Publishing
Journal of Optics
J. Opt. **27** (2025) 045609 (10pp)
https://doi.org/10.1088/2040-8986/adc141

Quantum inspired 3D pendulum beams

V Rodríguez-Fajardo[1,2,*], **T P Nguyen**[1] **and E J Galvez**[1,*]

[1] Department of Physics and Astronomy, Colgate University, 13 Oak Drive, Hamilton, NY 13346, United States of America
[2] Present address: Departamento de Fisica, Universidad Nacional de Colombia, Carrera 30 No. 45-03, Bogotá 111321, Colombia

E-mail: vrodriguezf@unal.edu.co and egalvez@colgate.edu

Received 31 January 2025, revised 6 March 2025
Accepted for publication 17 March 2025
Published 27 March 2025

Abstract

The technologies used in the manipulation of light can be used to do analogue simulations of physical systems with wave-like equations of motion. This analogy is maximized by the use of all the degrees of freedom of light. The Helmholtz equation in physical optics and the Schödinger equation in quantum mechanics share the same mathematical form. We use this connection to prepare non-diffracting optical beams representing the spatial and temporal dynamics of a nonlinear physical system: the quantum pendulum. By using the propagation coordinate to represent time in the quantum problem, we are able to analogue-simulate quantum wavepacket dynamics. These manifest themselves in novel optical beams with rich three-dimensional structures, such as rotation and sloshing of the light's intensity as it propagates. Our experimental results agree very well with the predictions from quantum theory, thus demonstrating that our system can be used as a platform to simulate the quantum pendulum dynamics. This three-dimensional light-sculpting capability has the potential to impact fields such as manipulation with light and imaging.

Keywords: structured light, quantum mechanics, pendulum

1. Introduction

Analogies in physics have been recognized as useful tools for investigating otherwise (nearly) inaccessible systems [1]. For instance, optical analogies have been used for ultra-fast signal processing [2], studying three-dimensional networks dynamics [3] and gravitational phenomena at astronomical scale [3–5]. The parallels between the Schrödinger equation and the Helmholtz equation in light propagation are well-known for the study quantum-light analog problems [6]. In particular, we are interested in the so-called pendulum beams [7, 8], that bridge between the quantum planar pendulum and Mathieu beams. The latter are a relatively new family of propagation invariant light beams [9] that have been used, among others, for 3D micro-particle assembly [10] and micro-cages fabrication [11]. The former was first studied from a theoretical perspective by Condon considering a gravitational potential [12], and today has found applications in biosensing [13]. It is particularly relevant in molecular physics, where it constitutes a physically reasonable system to model the rotational dynamics of molecular systems, which constitute a key witness of inter- and intra-molecular interactions [14]. Specifically, it has been used to model internal rotation and molecular orientation in spectroscopy [15, 16] and coherent control [17, 18]. The Mathieu equation that arises in the quantum solution of the problem is the basis for the implementation of the transmon qubit in the superconducting Josephson-junction system [19].

While the eigenfunctions of the planar quantum non-linear pendulum have been theoretically studied [20, 21] and experimentally by analogy using optical beams [8], its dynamic behavior is less explored, except for the two limiting cases of the harmonic oscillator and the free rotor. Theoretical studies investigate the dynamics of coherent superpositions [14, 22],

* Authors to whom any correspondence should be addressed.

being of particular interest the observation of quantum revivals [23–26], in which an initially localized quantum state spreads out to be later reformed so that the wave packet relocalizes [27]. Directly observing these quantum systems' dynamical behavior is very challenging, if possible, in most real systems. Hence, there is an interest in experimentally investigating them by analogy using other more accessible systems.

In addition, the use of the propagation coordinate creates new three-dimensional structures that can give rise to novel light patterns for imaging and manipulation. Various recreations of this type have been made with Gaussian beams, such as knots of vortex lines [28, 29] and Möbius patterns of polarization [30–32]. These knots have been discussed as potential carriers of information [33]. The selection of the propagation vectors in pulsed beams leads to 3D beams in space and time [34]. In the case of continuous-wave beams, superpositions of non-diffracting modes constitute a platform for manipulating the angular spectrum of the light to render rotations [35] and the generation of 3D caustic patterns [36]. Manipulation of the angular spectrum can be used as a laboratory astrophysics platform to study gravitational lensing [5].

In this work, we use quantum dynamics to define the 3D structure of the light. We propose and experimentally demonstrate an optical system that prepares coherent superpositions of Mathieu beams and uses the propagation coordinate to represent time in the dynamics of the quantum planar nonlinear pendulum. In doing so we create static 3D patterns of light intensity that represent the temporal evolution of a physical system. In section 2, we present the mathematical description of the problem from the quantum-mechanical and beam-mode perspectives. It is followed by the experimental procedure in section 3. In section 4, we present the results of three distinct quantum-dynamical cases, where the optical beams represent quantum wavepackets that illustrate the quantum rotor, the swinging pendulum and the non-classical double-pendulum. Discussion and conclusions are given in section 5.

2. Mathematical framework

Mathieu functions were first introduced to describe the vibrational modes of an elliptical membrane [37]. Since then, they have found applications in various fields of physics [38], including the description of the planar quantum pendulum [12] and, in physical optics, Mathieu beams [9]. We are interested in the connection between these two apparently distinct systems. Previously, we were interested in how non-diffracting 2D optical patterns represented the quantum problem, which also showed that the patterns in the far field were proportional to the quantum probabilities for the pendulum at a fixed time [8]. In this work, we create a 3D optical beam that represents the quantum problem for a range of times simultaneously, where the propagation direction serves as time in the quantum system. In this section, we outline how we set up the superposition of optical modes to mimic the time evolution of the quantum pendulum in 3D.

2.1. Quantum pendular systems

The behavior of a particle free to move along a ring and immersed in a periodic potential is a problem of interest in chemistry [39]. This is the case, for instance, of the methyl groups in Ethane (C_2H_6) and the $PtCl_6$ complex in Potassium hexachloroplatinate (K_2PtCl_6) [39]. For these systems, the potential is of the form $V=\frac{V_0}{2}(1+\cos m\theta)$ [22], where V_0 is the height of the barrier, m depends on the symmetry of the molecule, and θ represents the angular position of the particle. As an example, figure 1(a) shows the potential for ethane ($m=3$). The eigenfunctions of the system are found by solving the time–independent Schrödinger equation

$$\left(-\frac{\hbar^2}{2I}\frac{\mathrm{d}^2}{\mathrm{d}\theta^2}+\frac{V_0}{2}(1+\cos m\theta)\right)\psi=E\psi\,, \tag{1}$$

where I is the moment of inertial of the particle, E the energy eigen-values and ψ the wave-functions. By defining the adimensional scaled energies $U_0=\frac{2IV_0}{\hbar^2}$ and $\epsilon=\frac{2IE}{\hbar^2}$ as well as doing the change of variable $m\theta=2\eta$, equation (1) becomes

$$\frac{\mathrm{d}^2\psi}{\mathrm{d}\eta^2}+(a-2q\cos 2\eta)\,\psi=0\,, \tag{2}$$

where $a=\frac{4}{m^2}\left(\epsilon-\frac{U_0}{2}\right)$ and $q=\frac{U_0}{m^2}$. This equation is known as the ordinary (or angular) Mathieu equation and its solutions as the ordinary Mathieu functions [40]. The latter are divided into first-kind solutions, which are periodic and stable; and second-kind solutions, which are non-periodic and stable, or unstable.

The case $m=1$ corresponds to the pendulum. Given the symmetry of the physical system, we are only interested in the solutions of the first kind, for which q is real. These solutions are divided into two independent families with even or odd parity, and π- or 2π-periodicity [41]. Each family forms a countably infinite set of solutions $\{A_n[\eta]\}_{n\in\mathbb{Z}_{\geq 0}}$. In this case, the values of a in equation (2) are its eigenvalues, which are real, depend on the value of q, and are denoted as a_n and b_n for even and odd solutions, respectively. Moreover, since our system requires solutions with periodicity 2π in θ, we continue only with solutions with period π in η, which corresponds to even n. Specifically, they are the cosine- and sine-elliptical functions

$$\psi[\eta]=A_n[\eta]=\begin{cases}\mathrm{ce}_n[\eta;q] & n=0,2,4,\ldots\\ \mathrm{se}_n[\eta;q] & n=2,4,6,\ldots\end{cases}. \tag{3}$$

Figure 1(b) shows the first eleven solutions, each displaced to its scaled energy level and adjusted in magnitude for better visualization. The even and odd solutions are drawn as continuous and dotted lines, respectively. The corresponding potential barrier is drawn as a thick orange line for reference. For $m=1$, $q=U_0$ is the scaled energy of the potential barrier. The scaled energy levels of the eigensolutions of the system are given by

$$\epsilon_n^e=\frac{a_n}{4}+\frac{q}{2}\,,\qquad\text{and}\qquad\epsilon_n^o=\frac{b_n}{4}+\frac{q}{2}\,. \tag{4}$$

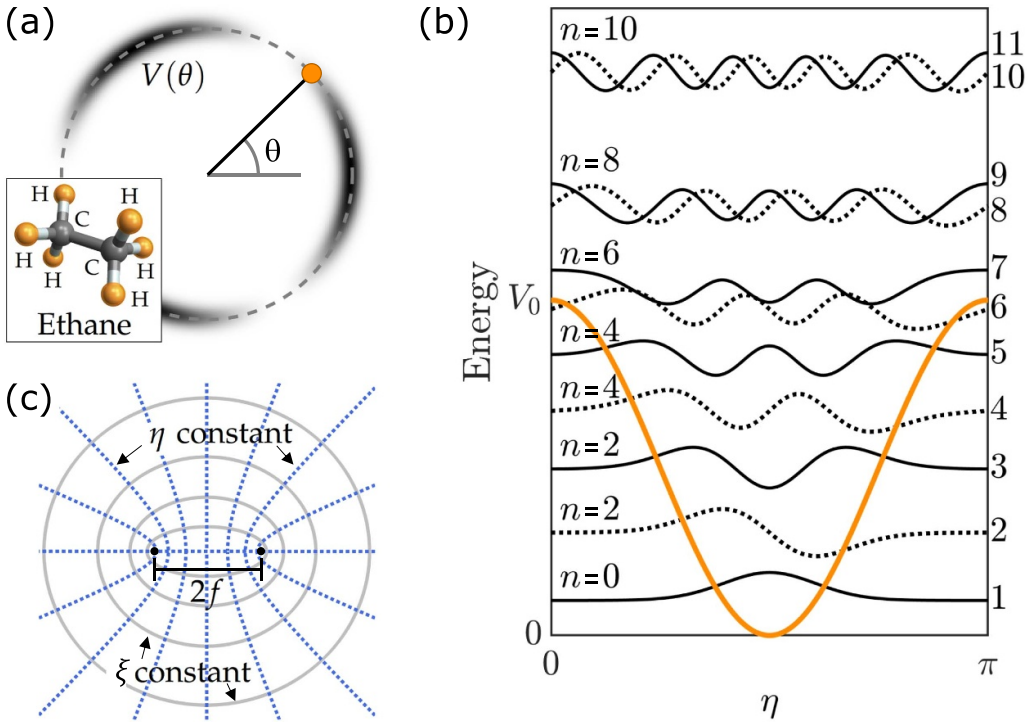

Figure 1. (a) Gray-scale representation of the electrostatic potential $V(\theta)$ for a methyl group in Ethane (C_2H_6). (b) First eleven eigenfunctions (equation (3)) for a non-linear quantum pendulum, drawn as continuous and dotted lines for even and odd states, respectively. Each function has been centred on the state's energy along the vertical axis and magnified for better visualization. (c) The elliptic coordinate system with interfocal separation $2f$. Continuous gray lines and dotted blue lines represent radial (ξ) and angular (η) coordinate lines, respectively.

Above the barrier, the difference between the scaled energies of even and odd solutions for energy levels decreases with increasing n to become nearly degenerate [41].

2.2. Pendulum beams

In light, Mathieu functions appear as solutions to the 2-dimensional Helmholtz equation for non-diffracting beams in elliptical coordinates, resulting in Mathieu beams [9]. Elliptical coordinates (ξ,η) are defined by

$$\begin{aligned} x &= f\cosh\xi\cos\eta \\ y &= f\sinh\xi\sin\eta \end{aligned}, \tag{5}$$

where $\xi\in[0,\infty)$ and $\eta\in[0,2\pi)$ are the radial- and angular-like variables, respectively. Figure 1(c) shows that contour lines of constant radial coordinate ξ are ellipses, and contour lines of constant angular coordinate η are hyperbolas. $2f$ is the separation between the two foci of the two types of curves. Expressed in elliptical coordinates, the Helmholtz equation takes the form

$$\frac{2}{f^2\left(\cosh^2 2\xi-\cos^2 2\eta\right)}\left(\frac{\partial^2}{\partial\xi^2}+\frac{\partial^2}{\partial\eta^2}\right)u+k_t^2u=0\,, \tag{6}$$

where k_t is the propagation constant in the transverse plane defined through $k^2=k_t^2+k_z^2$, with $k=\frac{2\pi}{\lambda}$ the wavevector and λ the wavelength. Equation (6) is solved following the method of separation of variables by making $u=A(\eta)R(\xi)$, yielding the ordinary (or angular) and modified (or radial) Mathieu differential equations

$$\frac{\mathrm{d}^2A[\eta]}{\mathrm{d}\eta^2}+(a-2q\cos 2\eta)A[\eta]=0\,, \tag{7}$$

$$\frac{\mathrm{d}^2R[\xi]}{\mathrm{d}\xi^2}-(a-2q\cosh 2\xi)R[\xi]=0\,, \tag{8}$$

where a is a separation constant and

$$q=\frac{f^2k_t^2}{4}\,. \tag{9}$$

The angular-elliptical solutions of equation (7) are identical to the quantum solutions described in section 2.1. The radial-elliptical solutions of equation (8) are expressed in terms of even and odd Bessel functions of the first kind, Je_n and Jo_n. They can be easily calculated from the angular solutions since equation (8) becomes equation (7) by making $\xi=\mathrm{i}\eta$. Thus, the modified Mathieu functions of the first kind are given by [40, 42]

$$R_n[\xi]=\begin{cases}\mathrm{Je}_n[\xi;q]=\mathrm{ce}_n[\mathrm{i}\xi;q] & n=0,1,2,\ldots\\ \mathrm{Jo}_n[\xi;q]=-\mathrm{i}\,\mathrm{se}_n[\mathrm{i}\xi;q] & n=1,2,3,\ldots\end{cases}. \tag{10}$$

Ideal non-diffracting Mathieu beams are then given by

$$\begin{cases}M_n^e[\xi,\eta;q]=\mathrm{Je}_n[\xi;q]\,\mathrm{ce}_n[\eta;q] & n=0,1,2,\ldots\\ M_n^o[\xi,\eta;q]=\mathrm{Jo}_n[\xi;q]\,\mathrm{se}_n[\eta;q] & n=1,2,3,\ldots\end{cases}. \tag{11}$$

However, these are not experimentally realizable because they are made of plane waves of infinite energy. Fortunately, we can overcome this by multiplying them by a Gaussian term, such that at the waist plane $u_0 = \exp(-r^2/w_0^2) M_n^{e,o}[\xi,\eta;q]$, where w_0 is the Gaussian width. The propagated beam is given by [43]

$$u[\mathbf{r}] = MG_n^{e,o}[\xi,\eta,z;q] = \frac{\mathrm{e}^{\mathrm{i}kz}}{\mu}\mathrm{e}^{-\mathrm{i}\frac{k_t^2}{2k}\frac{z}{\mu}}\mathrm{e}^{-\frac{r^2}{\mu w_0^2}} M_n^{e,o}[\xi,\eta;q]\,, \tag{12}$$

where $\mu = \mu[z] = 1 + \mathrm{i}z/z_\mathrm{R}$, with $z_\mathrm{R} = kw_0^2/2$ being the Rayleigh range of the Gaussian beam [44]. Equation (12) describes the Mathieu–Gauss beam, which is a solution of the homogeneous Helmholtz equation in the paraxial regime.

Crucially, because equations (7) and (2) have the same form, we can establish a direct connection between the quantum non-linear pendulum and Mathieu beams. Remarkably, their transverse Fourier spectrum is proportional to the quantum probabilities of the pendulum, as has been theoretically proposed [7] and experimentally demonstrated [8].

2.3. 3D quantum wavepackets

In this work, we extend the analogy between the quantum pendulum and pendulum beams from the stationary to the dynamic situation. For a time–independent Hamiltonian, the time evolution of a superposition of even and odd eigenfunctions is given by

$$\Psi[\eta,t] = \sum_{p=1}^{N}\left\{\psi_{2p}^{e}[\eta]\exp\left(\mathrm{i}\frac{E_{2p}^{e}}{\hbar}t\right) + \mathrm{i}\psi_{2p}^{o}[\eta]\exp\left(\mathrm{i}\frac{E_{2p}^{o}}{\hbar}t\right)\right\}, \tag{13}$$

where the state quantum number is $n = 2p$. The summation starts at $p = 1$ to pair even with odd functions since odd modes are only defined for $n \geqslant 2$. The superposition consists of $2N$ modes, all sharing the same value of q, the height of the potential barrier.

The first step in the optical implementation is to create superpositions of Mathieu beams

$$U[\mathbf{r};q] = \sum_{p=1}^{N}\left(MG_{2p}^{e}[\xi,\eta,z;q] + \mathrm{i}MG_{2p}^{o}[\xi,\eta,z;q]\right), \tag{14}$$

where the terms in the summation represent Helical Mathieu–Gauss beams. These are elliptical in shape, containing n optical vortices linearly arrayed along the semi-major axis of the ellipse. The phase of the mode increases following an elliptical trajectory and carries orbital angular momentum [45]. We complete the implementation of equation (13) by specifying different propagation vectors for each value of p

$$U[\mathbf{r}] = \sum_{p=1}^{N}\left\{M_{2p}^{e}[\xi,\eta;q]\exp\left(\mathrm{i}\frac{\left(k_{t_{2p}}^{e}\right)^2}{2k}z\right) + \mathrm{i}M_{2p}^{o}[\xi,\eta;q]\exp\left(\mathrm{i}\frac{\left(k_{t_{2p}}^{o}\right)^2}{2k}z\right)\right\}\mathrm{e}^{\mathrm{i}kz}\mathrm{e}^{-\frac{r^2}{w_0^2}}. \tag{15}$$

To make an exact parallel with equation (13) we scale $k_{t_{2p}}$ to be proportional to the energy of the quantum states of the pendulum:

$$k_{t_{2p}}^{e,o} = \sqrt{\frac{E_{2p}^{e,o}}{E_{2N}^{e}}}k_{t_{2N}}^{e} = \sqrt{\frac{\epsilon_{2p}^{e,o}}{\epsilon_{2N}^{e}}}k_{t_{2N}}^{e}\,. \tag{16}$$

We note that to reach this simplified dependence with z, we make w_0 in equation (12) sufficiently large so that the approximation $\mu(z) \approx 1$ is valid along the experimental propagation range we measured over, as detailed in the next section. In the ray description of these non-diffracting modes, equation (15) entails a superposition of non-diffracting modes with differing conical angles.

3. Experimental details

In figure 2(a) we show a schematic of the optical setup used in the laboratory. A light beam from a He–Ne laser was expanded and collimated using a telescope composed of lenses L_1 and L_2, with focal lengths $f_1 = 5$ cm and $f_2 = 75$ cm, respectively. A half-waveplate in combination with a fixed linear polarizer (LP) was used to control the power of the beam.

The beam was subsequently steered to a phase-only liquid-crystal spatial light modulator (SLM: Hamamatsu model LCOS, with 800×600 pixels of size $20\,\mu$m), where a computer-generated hologram was encoded. Holograms included amplitude modulation [46], a blazed phase grating, and a correction to counteract aberrations of the optical system [47]. Figure 2(b) shows the hologram for one of the cases we studied, with the grating periodicity increased for illustration.

The SLM plane was imaged using lenses L_3 and L_4 (with focal lengths $f_3 = 75$ cm and $f_4 = 25$ cm, respectively) in a 4f configuration. The conjugate plane of the SLM is shown by the dotted lines in figure 2(a). Undesired diffraction orders were filtered using a spatial filter (SF) located at the focal plane of L_3. A digital camera (CAM_1: Thorlabs DCC1645C with 3.6 cm pixel size) mounted on a motorized translation stage (Thorlabs LTS300) was used to acquire images of light beams along the optical path from the image plane, at $z = 0$, to a distance $z = 30$ cm.

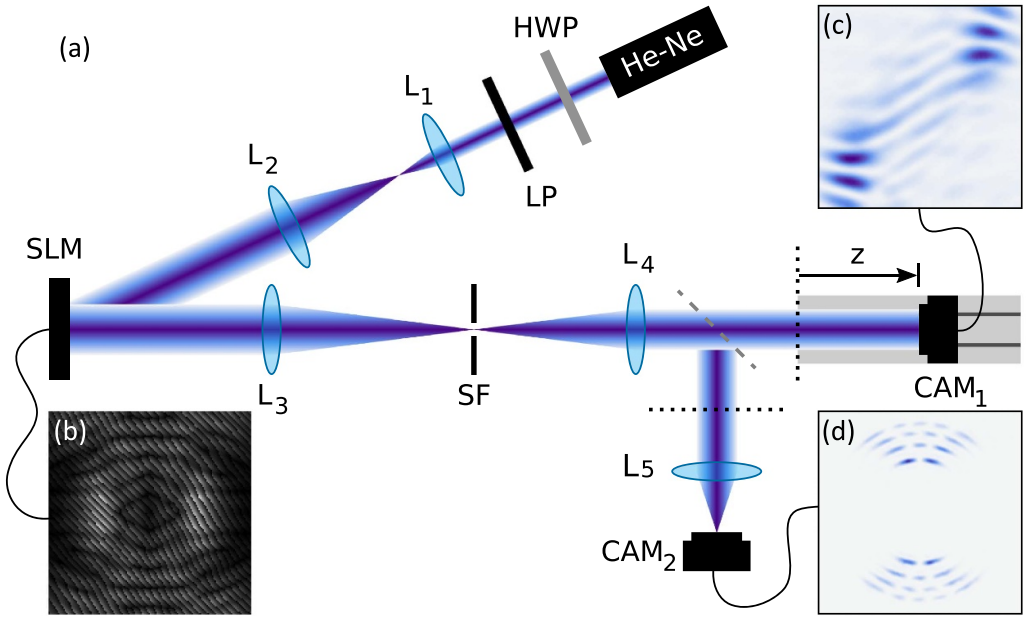

Figure 2. (a) Schematic diagram of the implemented experimental setup. A liquid crystal spatial light modulator (SLM) was illuminated with an expanded and collimated He–Ne laser light beam ($\lambda = 633$ nm). The spatial mode of the beam was created by a hologram displayed on the SLM, as shown in (b). A 4-f system of lenses relayed the beam further downstream, where images of the propagating beam were taken using a digital camera on a rail (CAM_1), as shown in (c). A second camera (CAM_2) was placed at the Fourier plane of the SLM to capture images of the far-field beam, shown in (d). Unwanted diffraction orders were removed by using a spatial filter (SF) and power was controlled using a half-wave plate (HWP) / LP (LP) combination.

We used a mirror on a flip mount (depicted as a dashed gray line after L_4) to optionally redirect the beam towards a lens L_5, which Fourier-transformed the image plane onto a second digital camera (CAM_2: Thorlabs DCC1545M with 5.2 μm pixel size). Accessing the Fourier plane allowed us to define the maximum transversal wavevector our system could sustain, which was limited mainly by the size of the SF in the beam's path. The latter was made as large as possible, while also filtering out other diffraction orders. We choose the maximum value of $k^e_{t_{2N}} = 15 \times 10^3$ m^{-1} for all our measurements. The complete data acquisition process was automated using custom-made MATLAB scripts, including driving the translation stage and capturing the images.

We created superpositions of Mathieu beams following equation (15). In all cases, we used a Gaussian width $w_0 =$ 5 mm that fit well within the SLM, which corresponds to a Rayleigh range $z_R \sim 124$ m. This leads to $\mu = 1 + iz/z_R \approx 1$ for the range of the experiments, with a maximum propagation distance $z = 0.3$ m (see equation (12)). Since all modes must share the same parameter q, but have different k_t, it was necessary to modify the semi-focal separation f in the definition of elliptical coordinates (equation (5)) for each mode to ensure that equation (9) was satisfied. Mathieu functions were calculated using adaptations of the MATLAB libraries created by Gutiérrez-Vega [41]. This setup enables the simulation of other physical systems with distinct dynamics by changing the hologram displayed without modifying the optical setup.

4. Results

A key difference between the quantum pendulum and Mathieu beams is that while the first one is a one-dimensional system, the second one is two-dimensional. That is, the quantum probability encoded in the angular-elliptical coordinate is distributed along the radial-elliptical coordinate of the beam mode, as can be appreciated in figure 2(c). In addition, for $m = 1$, $\theta = 2\eta$, so there is a 1:2 mapping of the theoretical quantum probability for the pendulum to the intensity of the optical mode. That is, the optical mode corresponds to a variation in θ that goes from 0 to 4π in the captured image. This makes the pattern on the top half of the image repeat on the lower half. This feature is particularly evident in the quantum superposition shown, which is asymmetric, representing the pendulum at a turning point of its oscillation.

In the far field, the radial component for a stationary state, expressed in terms of Bessel functions, collapses into a delta function of the radial (polar) coordinate. Optically, this corresponds to a single ring with a radius proportional to the transverse wave-vector, with the angular solution modulating the intensity along the ring [7, 48]. This has been demonstrated experimentally to be proportional to the quantum probability $|\psi[\eta]|^2$ [8]. However, in the case of a superposition of modes $U[\mathbf{r}; q]$ (states $\Psi[\eta, t]$) of different transverse wave-vectors k_{tn} (energies E_{tn}), the far-field pattern consists of several rings with a radius that depends on k_{tn} (E_{tn}), as shown in figure 2(d). The top half of this image and mirror-inverted lower half are

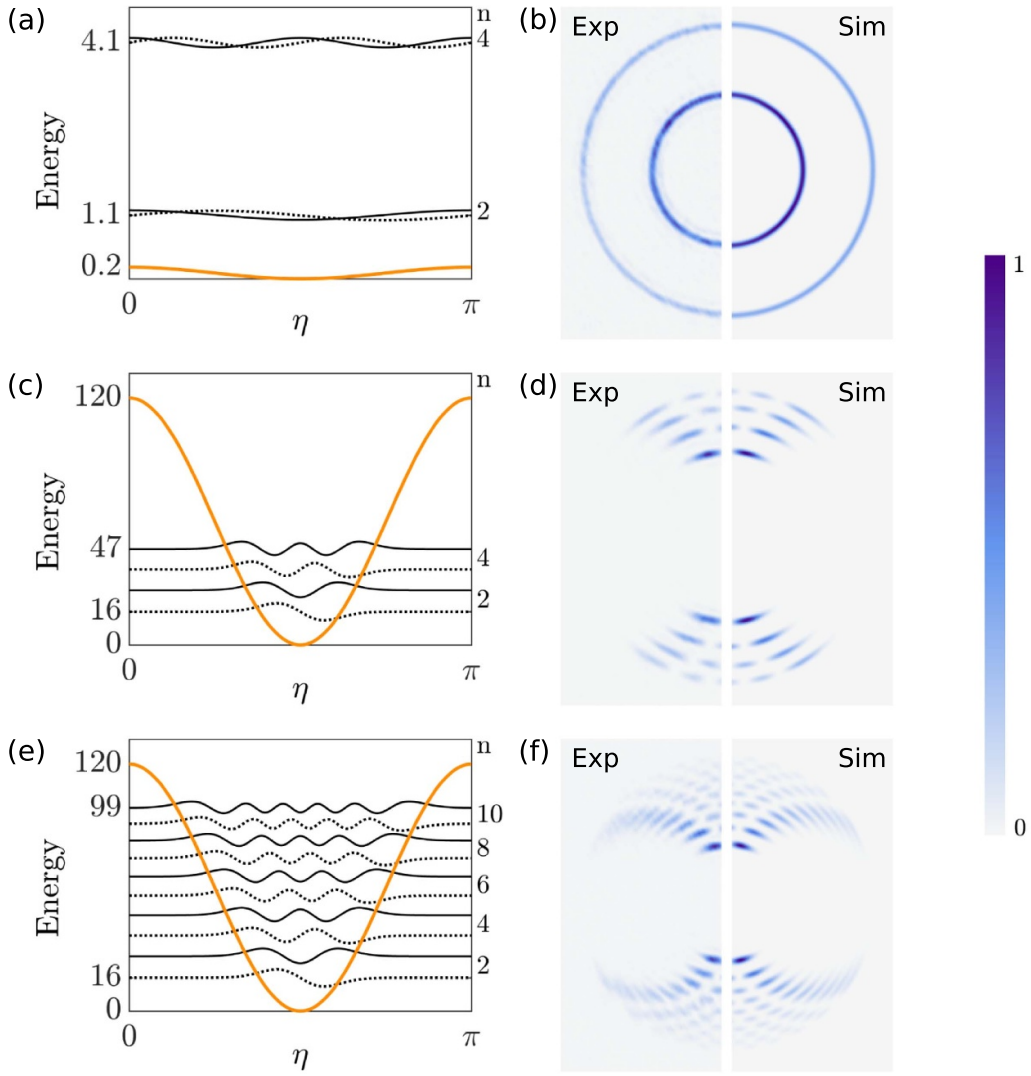

Figure 3. Energy levels diagrams of the modes in the superposition for (a) a rotor or unbounded pendulum ($q = 0.2$, $n = 2, 4$), (c) an oscillating pendulum ($q = 120$, $n = 2, 4$), and (e) a double pendulum ($q = 120$, $n = 2, 4, 6, 8, 10$), and corresponding experimental (left) and numerically simulated (right) Fourier transform of the optical beam for the same cases in (b), (d) and (f), respectively. Here, we have taken advantage of the symmetry of the intensity profiles, and show only the left (right) parts of the experimental (simulated) images.

an analogue form of the energy-level diagram of the states of the superposition, modulated by their respective quantum probabilities. The specific case of figure 2(d) corresponds to the superposition of four states. Focusing on the upper half of the insert, the ordering of states is, from lower to upper, $n = 2$ (odd), $n = 2$ (even), $n = 4$ (odd), and $n = 4$ (even). The odd (even) parity of each state is evident by a node (antinode) at the centres of the respective patterns. The image is a striking analogue-optical representation of a quantum energy-level diagram such as the one in figure 1(b).

4.1. Cases

We present three cases of superpositions with distinct dynamic behavior.

4.1.1. Case I: the pendulum rotor. This case corresponds to the unbounded pendulum, where the states involved in the superposition are above the potential barrier, as seen in figure 3(a). In this case, the superposition consists of four modes ($N = 2$), all sharing the parameter $q = 0.2$. Each wavefunction is drawn at a height that corresponds to its energy level, and magnified in amplitude for better visualization. Even and odd modes are drawn as continuous and dotted lines, respectively. The height of the potential barrier is given by q. The experimental and numerically simulated Fourier transforms of the optical superposition are shown in figure 3(b), where taking advantage of the symmetry of the images, we compare the two, with the left half being the experimental image and the right half the simulation. Only two rings are seen since the even and odd states of the same n are nearly

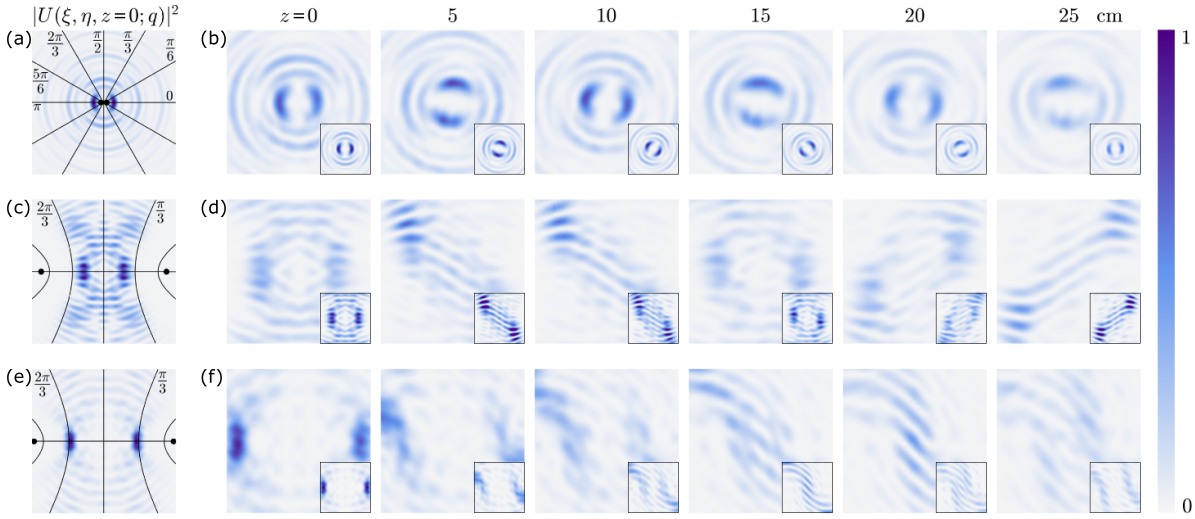

Figure 4. Analytically computed intensity for (a) an unbounded pendulum (a rotor), (c) an oscillating pendulum, and (e) a double pendulum. Example hyperbolas of constant angular-elliptical coordinate η are shown for reference, along with the two foci of the coordinate system. (b), (d), (f) Corresponding experimental images of the propagated beam from $z=0$ to $z=25$ cm in steps of $\Delta z=5$ cm Insets present the numerically simulated light beams.

degenerate. The rings are not modulated in intensity because the probability of finding the rotor is the same for all angles.

The analytically calculated mode at $z=0$ is shown in figure 4(a), along with the contour lines for the angular-elliptical coordinate, in multiples of $\eta=\frac{\pi}{6}$. Because $q\to 0$, elliptical coordinates converge to polar ones, and these lines resemble radial lines. The experimental images of the propagating beam are shown in figure 4(b) as a sequence of images. They include inserts with numerically simulated calculations using the first Rayleigh–Sommerfeld diffraction solution [49]. Upon propagation, the whole pattern rotates counter-clockwise in a rotor-like fashion, such that its size slightly increases and its shape is mostly maintained. For instance, the two predominant lobes in the middle rotate around the centre while their relative position is unchanged. Simulated images showcase the same type of behavior, although the rotation rate is slower. The difference may be due to a systematic error in the imaging system. Similar patterns and rotation dynamics have been previously observed using Bessel beams [50, 51] and tornado waves [52].

Notice also that while there are arcs of high intensity at low radius, other arcs at larger radii are offset. A long-term examination of this problem shows that the offset intensities are due to temporal recurrences. That is, the states involved in the superposition can be in phase, showing a single rotor, but can also double their period for other phase combinations. The sequence mildly shows the combination of these two situations.

4.1.2. Case II: the oscillating pendulum. The second case corresponds to the oscillating pendulum. Figures. 3(c) and (d) show, respectively, the energy-level diagram of the four states involved in the superposition and the Fourier transform of the optical beam. The state parameters for this case are $N=2$ and $q=120$. This is also the example shown in figures 2(b)–(d). In this case, the states are all relatively low in the potential well and are nondegenerate. Thus, the Fourier transform of the mode consists of four rings with their intensity modulated by the corresponding probability for each state ($|\psi(\eta)|^2$).

Figures 4(c) and (d) present, respectively, the analytical and measured images of the beam pattern for this case. The intensity of the beam shown starts symmetrically distributed with respect to $\eta=\frac{\pi}{2}$ at $z=0$. Subsequently, it shifts to one of the pendular turning points (angles) for $z=5$ cm and $z=10$ cm. After returning to be almost symmetrical at $z=15$ cm, the pendulum swings to the other turning point at $z=20$ cm and $z=25$ cm. This oscillation in the intensity distribution resembles the back-and-forth movement of a pendulum.

4.1.3. Case III: the double pendulum. A third case that we show consists of a non-classical version of the pendulum, which we call the double pendulum. It corresponds to a superposition of 10 states, with $N=5$ and $q=120$. This case is shown in figures 3(e) and (f). Since there are 10 modes in the superposition, all below the potential barrier, the energy diagram and image are more congested. As the energy of the state increases, the maximum elongation of the arc also increases, corresponding to larger pendular turning points. The non-classical aspect of the dynamics is evident in figures 4(e) and (f), where the quantum probability is localized at two distinct angles. The two bright lobes in the pattern move in opposite directions: towards the centre of the pattern at $z=5, 10, 15$ cm, across in the middle for $z\approx 20$ cm, to continue moving away from each other for $z=25$ cm. We interpret this as two pendulums moving in opposite directions in a coordinated fashion, a situation that has no analogy in the classical system for a single pendulum. It may resemble the case of two pendulum bobs that oscillate but collide elastically at the lower point of the oscillation.

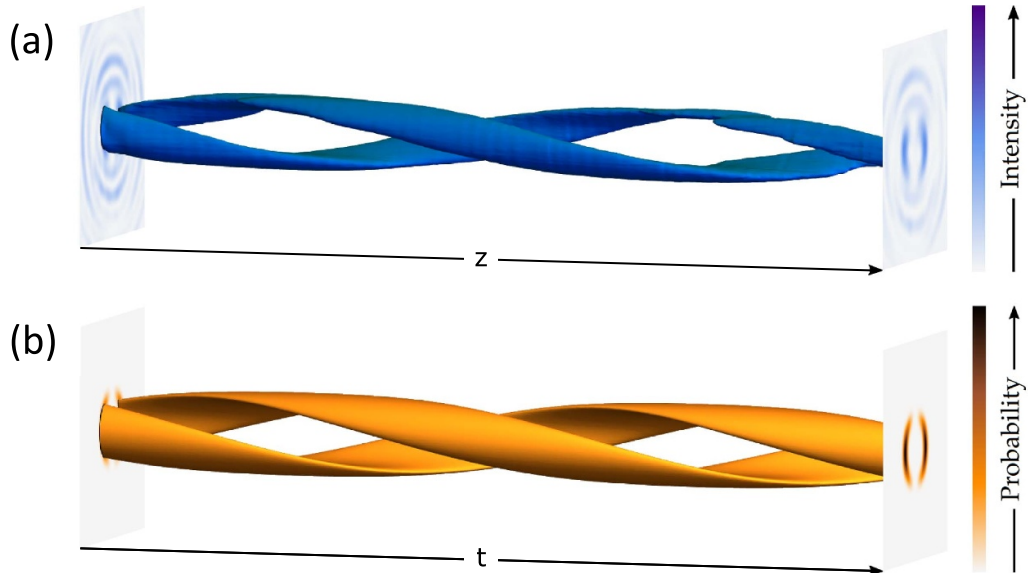

Figure 5. (a) Evolution in space of the corresponding three-dimensional intensity for a coherent superposition of modes representing a rotor (Case I in the text). (b) Computed evolution in time of the probability of the quantum pendulum.

4.2. 3D beams

We took data over a span of values of z to map the 3D shape of the beam. This is shown in figure 5(a) for Case I. It is a composite of the images taken stepwise along z. The graph of a surface representing the intensity of the beam illustrates the 3D character of the beam. The 2:1 mapping of the quantum probability into the beam mode results in a non-diffracting double helix, which for the span measured corresponds to one full revolution of the helix. In figure 1(b), we plot the analytically calculated beam, showing excellent agreement. We note that the helix shown is static in space, with its phase depending on the initial absolute phase of the superposition encoded onto the SLM. Changing this phase in real-time makes the helix rotate. Such a 3D pattern could be used in the optical transport of trapped particles in an optical tweezer as a form of an Archimedes screw.

5. Conclusions

In summary, we have developed an optical platform to study the dynamics of the quantum planar non-linear pendulum. We present a theoretical framework that supports the analogy and experimental results that confirm it. We presented three representative cases with distinct dynamical behavior, all exhibiting quantum-like traits. Our approach provides a reliable, versatile, and relatively easy-to-implement tool for mimicking a quantum system using a classical system: light beams. Thus, opening the possibility of investigating quantum systems by analogy. Interestingly, an optical analogy of the classical pendulum was recently reported [53], where a harmonic potential is considered and its typical oscillatory behavior observed, with the added advantage of observing the wave-particle duality of their so-called light particles.

Given the good performance of our platform, we anticipate that it could be used to simulate other systems governed by a Schrödinger equation that can be mimicked by the wave equation. One such system is the particle in a quartic potential, which is mimicked by accelerating parabolic beams [54]. Other examples include transmons [19], and oscillatory quantum-fluid polaritons [55]. In addition, it could also be used to introduce a wider range of audiences to concepts in quantum mechanics using a more visual approach. The images of the energy-level diagram specified by the corresponding quantum probabilities, shown in figures 2(d), 3(a),(c) and (e) are a pedagogical analogue illustration of the quantization of mechanical systems. Besides the potential as a platform for optical analogies, future research includes the investigation of optical knots in our three-dimensional optical pendulum beams and creating vector beams using them to investigate skirmions in propagation.

These 3D beams have potential for applications in particle manipulation with light. For example, the 3D helical pattern of figures 1(d) and (e), where an optical helix of intensity can be rotated for transporting trapped particles in either axial direction in a new optical version of Archimedes screw [56–58]. Other combinations of sloshing intensities could do similarly by rendering traveling waves of various types, opening possibilities for applications in light sculpturing and imaging.

Data availability statement

All data that support the findings of this study are included within the article (and any supplementary files).

Acknowledgments

This work was funded by the National Science Foundation Grant PHY-2011937. The authors thank A Forbes for useful discussions.

ORCID iDs

V Rodríguez-Fajardo https://orcid.org/0000-0003-3953-7430
E J Galvez https://orcid.org/0000-0003-0918-2245

References

[1] Oppenheimer R 1956 Analogy in science *Am. Psychol.* **11** 127–35
[2] Torres-Company V, Lancis J and Andrés P 2011 Space-time analogies in optics *Prog. Opt.* **56** 1–80
[3] Ehrhardt M, Keil R, Maczewsky L J, Dittel C, Heinrich M and Szameit A 2021 Exploring complex graphs using three-dimensional quantum walks of correlated photons *Sci. Adv.* **7** eabc5266
[4] Roger T, Maitland C, Wilson K, Westerberg N, Vocke D, Wright E M and Faccio D 2016 Optical analogues of the Newton-Schrödinger equation and boson star evolution *Nat. Commun.* **7** 13492
[5] Rodríguez-Fajardo V, Nguyen T P, Hocek K S, Freedman J M and Galvez E J 2023 Einstein beams and the diffractive aspect of gravitationally-lensed light *New J. Phys.* **25** 083033
[6] Marte M A M and Stenholm S 1997 Paraxial light and atom optics: the optical Schrödinger equation and beyond *Phys. Rev.* A **56** 2940–53
[7] Dennis M R and Ring J D 2013 Propagation-invariant beams with quantum pendulum spectra: from Bessel beams to Gaussian beam-beams *Opt. Lett.* **38** 3325
[8] Galvez E J, Auccapuclla F J, Qin Y, Wittler K L and Freedman J M 2021 Pendulum beams: optical modes that simulate the quantum pendulum *J. Opt.* **23** 024001
[9] Gutiérrez-Vega J C, Iturbe-Castillo M D and Chávez-Cerda S 2000 Alternative formulation for invariant optical fields: Mathieu beams *Opt. Lett.* **25** 1493
[10] Macdonald M *et al* 2010 Mathieu beams as versatile light moulds for 3D micro particle assemblies *Opt. Express* **18** 26084–91
[11] Wang C *et al* 2019 Femtosecond mathieu beams for rapid controllable fabrication of complex microcages and application in trapping microobjects *ACS Nano* **13** 4667–76
[12] Condon E U 1928 The physical pendulum in quantum mechanics *Phys. Rev.* **31** 891–4
[13] Das J, Gomis S, Chen J B, Yousefi H, Ahmed S, Mahmud A, Zhou W, Sargent E H and Kelley S O 2021 Reagentless biomolecular analysis using a molecular pendulum *Nat. Chem.* **13** 428–34
[14] Dimeo R M 2003 Visualization and measurement of quantum rotational dynamics *Am. J. Phys.* **71** 885–93
[15] Lin C C and Swalen J D 1959 Internal rotation and microwave spectroscopy *Rev. Mod. Phys.* **31** 841–91
[16] Hershbach D R 1959 Calculation of energy levels for internal torsion and over-all rotation. III *J. Chem. Phys.* **31** 91–108
[17] Friedrich B, Pullman D P and Herschbach D R 1991 Alignment and orientation of rotationally cool molecules *J. Phys. Chem.* **95** 8118–29
[18] Ramakrishna S and Seideman T 2007 Torsional control by intense pulses *Phys. Rev. Lett.* **99** 1–4
[19] Koch J, Yu T M, Gambetta J, Houck A A, Schuster D I, Majer J, Blais A, Devoret M H, Girvin S M and Schoelkopf R J 2007 Charge-insensitive qubit design derived from the Cooper pair box *Phys. Rev.* A **76** 042319
[20] Baker G L, Blackburn J A and Smith H J T 2002 The quantum pendulum: small and large *Am. J. Phys.* **70** 525–31
[21] Schmidt B and Friedrich B 2014 Supersymmetry and eigensurface topology of the planar quantum pendulum *Front. Phys.* **2** 1–16
[22] Leibscher M and Schmidt B 2009 Quantum dynamics of a plane pendulum *Phys. Rev.* A **80** 1–16
[23] Parker J and Stroud C R 1986 Coherence and decay of Rydberg wave packets *Phys. Rev. Lett.* **56** 717–9
[24] Yeazell J A and Stroud C R 1991 Observation of fractional revivals in the evolution of a Rydberg atomic wave packet *Phys. Rev.* A **43** 5153–6
[25] Bluhm R, Kostelecky V A and Porter J A 1996 The evolution and revival structure of localized quantum wave packets *Am. J. Phys.* **64** 944–53
[26] Doncheski M A and Robinett R W 2003 Wave packet revivals and the energy eigenvalue spectrum of the quantum pendulum *Ann. Phys., NY* **308** 578–98
[27] Robinett R W 2004 Quantum wave packet revivals *Phys. Rep.* **392** 1–119
[28] Berry M V and Dennis M R 2001 Knotted and linked phase singularities in monochromatic waves *Proc. R. Soc.* A *457* 2251–63
[29] Leach J, Dennis M R, Courtial J and Padgett M J 2004 Knotted threads of darkness *Nature* **432** 165–165
[30] Bauer T, Banzer P, Karimi E, Orlov S, Rubano A, Marrucci L, Santamato E, Boyd R W and Leuchs G 2015 Observation of optical polarization Möbius strips *Science* **347** 964–6
[31] Galvez E J, Dutta I, Beach K, Zeosky J J, Jones J A and Khajavi B 2017 Multitwist Möbius strips and twisted ribbons in the polarization of paraxial light beams *Sci. Rep.* **7** 13653
[32] Pisanty E, Machado G J, Vicuña-Hernández V, Picón A, Celi A, Torres J P and Lewenstein M 2019 Knotting fractional-order knots with the polarization state of light *Nat. Photon.* **13** 569–74
[33] Larocque H, D'Errico A, Ferrer-Garcia M F, Carmi A, Cohen E and Karimi E 2020 Optical framed knots as information carriers *Nat. Commun.* **11** 5119
[34] Kondakci H E and Abouraddy A F 2019 Optical space-time wave packets having arbitrary group velocities in free space *Nat. Commun.* **10** 929
[35] Shen Y, Yang X, Naidoo D, Fu X and Forbes A 2020 Structured ray-wave vector vortex beams in multiple degrees of freedom from a laser *Optica* **7** 820–31
[36] Zannotti A, Denz C, Alonso M A and Dennis M R 2020 Shaping caustics into propagation-invariant light *Nat. Commun.* **11** 3597
[37] Mathieu E 1868 Mémoire sur le mouvement vibratoire d'une membrane de forme elliptique *J. Math. Pure. Appl.* **13** 137–203
[38] Ruby L 1996 Applications of the Mathieu equation *Am. J. Phys.* **64** 39–44
[39] Baker G L and Blackburn J A 2005 *The Pendulum: A Case Study in Physics* (Oxford University Press) ch 8
[40] McLachlan N W 1951 *Theory and Application of Mathieu Functions* (Oxford University Press)
[41] Gutiérrez-Vega J C 2000 Formal analysis of the propagation invariant optical fields in elliptic coordinates *PhD Thesis* Instituto Nacional de Astrofísica, Óptica y Electrónica
[42] Gutiérrez-Vega J C, Rodríguez-Dagnino R M, Meneses-Nava M A and Chávez-Cerda S 2003 Mathieu functions, a visual approach *Am. J. Phys.* **71** 233–42

[43] Gutiérrez-Vega J C and Bandres M A 2005 Helmholtz–Gauss waves *J. Opt. Soc. Am.* A **22** 289
[44] Siegman A E 1986 *Lasers* (University Science Books)
[45] Chávez-Cerda S, Gutiérrez-Vega J C and New G H C 2001 Elliptic vortices of electromagnetic wave fields *Opt. Lett.* **26** 1803
[46] Bolduc E, Bent N, Santamato E, Karimi E and Boyd R W 2013 Exact solution to simultaneous intensity and phase encryption with a single phase-only hologram *Opt. Lett.* **38** 3546
[47] Jesacher A, Schwaighofer A, Fürhapter S, Maurer C, Bernet S and Ritsch-Marte M 2007 Wavefront correction of spatial light modulators using an optical vortex image *Opt. Express* **15** 5801
[48] Gutiérrez-Vega J C, Iturbe-Castillo M D, Ramírez G A, Tepichín E, Rodríguez-Dagnino R M, Chávez-Cerda S and New G H C 2001 Experimental demonstration of optical Mathieu beams *Opt. Commun.* **195** 35–40
[49] Goodman J W 2005 *Introduction to Fourier optics* (Roberts & Company)
[50] Kotlyar V V, Khonina S N, Skidanov R V and Soifer V A 2007 Rotation of laser beams with zero of the orbital angular momentum *Opt. Commun.* **274** 8–14
[51] Schulze C, Roux F S, Dudley A, Rop R, Duparré M and Forbes A 2015 Accelerated rotation with orbital angular momentum modes *Phys. Rev.* A **91** 1–8
[52] Brimis A, Makris K G and Papazoglou D G 2020 Tornado waves *Opt. Lett.* **45** 280
[53] Jia J *et al* 2023 Pendulum-type light beams *Optica* **10** 90–96
[54] Bandres M A 2008 Accelerating parabolic beams *Opt. Lett.* **33** 1678–80
[55] Tosi G, Christmann G, Berloff N G, Tsotsis P, Gao T, Hatzopoulos Z, Savvidis P G and Baumberg J J 2012 Sculpting oscillators with light within a nonlinear quantum fluid *Nat. Phys.* **8** 190–4
[56] Hadad B, Froim S, Nagar H, Admon T, Eliezer Y, Roichman Y and Bahabad A 2018 Particle trapping and conveying using an optical Archimedes' screw *Optica* **5** 551–6
[57] Mohammadnezhad M, Abdulkareem S S and Hassanzadeh A 2022 Creation of rotating spiral structures using interfering Bessel beams for optical manipulation *Opt. Lett.* **47** 4024
[58] Ding Z and Yu Y 2024 Archimedes spiral beam: composite of a helical-axicon generated Bessel beam and a Gaussian beam *J. Opt. Soc. Am.* A **41** 874–80